AIP Applied Physics Letters

Photothermally excited force modulation microscopy for broadband nanomechanical property measurements

Ryan Wagner and Jason P. Killgore

Citation: Applied Physics Letters **107**, 203111 (2015); doi: 10.1063/1.4935982
View online: http://dx.doi.org/10.1063/1.4935982
View Table of Contents: http://scitation.aip.org/content/aip/journal/apl/107/20?ver=pdfcov
Published by the AIP Publishing

Photothermally excited force modulation microscopy for broadband nanomechanical property measurements

Ryan Wagner[a)] and Jason P. Killgore
Material Measurement Laboratory, National Institute of Standards and Technology, Boulder, Colorado 80305, USA

(Received 14 October 2015; accepted 4 November 2015; published online 18 November 2015)

We demonstrate photothermally excited force modulation microscopy (PTE FMM) for mechanical property characterization across a broad frequency range with an atomic force microscope (AFM). Photothermal excitation allows for an AFM cantilever driving force that varies smoothly as a function of drive frequency, thus avoiding the problem of spurious resonant vibrations that hinder piezoelectric excitation schemes. A complication of PTE FMM is that the sub-resonance cantilever vibration shape is fundamentally different compared to piezoelectric excitation. By directly measuring the vibrational shape of the cantilever, we show that PTE FMM is an accurate nanomechanical characterization method. PTE FMM is a pathway towards the characterization of frequency sensitive specimens such as polymers and biomaterials with frequency range limited only by the resonance frequency of the cantilever and the low frequency limit of the AFM.
[http://dx.doi.org/10.1063/1.4935982]

The atomic force microscope (AFM) can provide nanoscale, spatially resolved mechanical property information. Usually, these measurements are performed at a single low frequency in the Hertz range,[1] or at a single high frequency determined by the resonance of the AFM cantilever, which is in the kHz to MHz range.[2] Due to its inherently large bandwidth, the AFM is well suited for nanometer-scale frequency-dependent characterization.[3,4] Such characterization will benefit applications where stresses vary over large time scales, while also providing a validation for property data measured with traditional AFM methods at high frequencies.

Force modulation microscopy[5] (FMM) is a sub-resonance continuous contact AFM technique that relates the cantilever vibration amplitude A to the tip-sample contact stiffness k. For optical beam detection,[6] A is the oscillation amplitude of the photodiode voltage, which is predominantly proportional to cantilever slope at the detection laser position. The value of k can be measured at any f from the low-frequency noise floor up to $\approx$10% of the first resonance of the cantilever. Of current AFM techniques, FMM serves as a promising starting point for characterization of frequency-dependent nanomechanical properties and has had success in characterizing frequency-dependent properties over frequency ranges from Hz to kHz.[3,7]

A challenge with extending FMM into higher frequency ranges is maintaining a constant or smoothly varying drive force as a function of drive frequency. Acoustic excitation,[8] where a piezoelectric element drives the base of the cantilever or the base of the sample, tends to excite spurious resonances.[9,10] These spurious resonances can be reduced, but not eliminated, with more-robust design of the sample or cantilever mounting system.[11] Nevertheless, methods that apply a force directly to the cantilever, such as photothermal excitation (PTE),[12] avoid many of the problems associated with acoustic excitation. PTE operates by focusing a second, drive laser onto the cantilever, as shown in Fig. 1(a). Oscillating the power of the PTE drive laser results in cantilever motion via a combination of local thermal gradients and bimorph bending.[13] For PTE, the maximum sub-resonance A will occur when the cantilever is freely vibrating far from the sample. For acoustic excitation with a piezoelectric actuator at the cantilever base, there is near zero sub-resonance response in free vibration and maximum response when in contact with a stiff surface. Fig. 1(b) shows a comparison of A versus f for PTE and acoustic excitation at the cantilever base where the sub-resonance A has been maximized. Both acoustic excitation and PTE exhibit a smooth cantilever response at low frequencies; however, at $f > 40$ kHz, spurious resonances affect the response of the acoustically driven system. The smooth

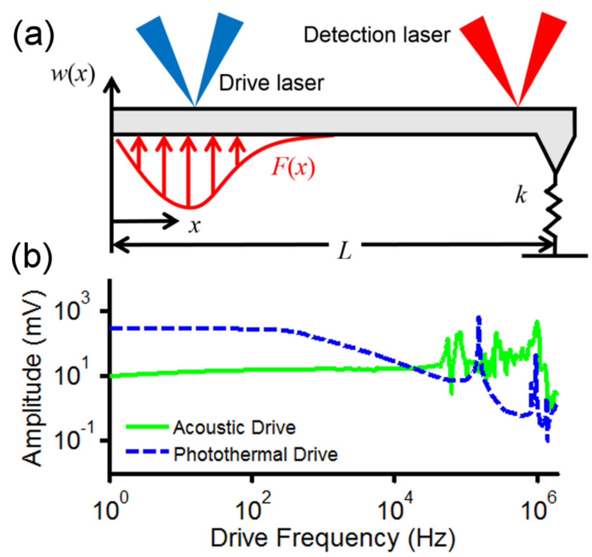

FIG. 1. (a) Photothermal excitation schematic and definition of variables for force modulation microscopy model. (b) Comparison of free photothermal frequency sweep and contact acoustic frequency sweep.

a)Electronic mail: ryan.wagner@nist.gov

frequency-dependent cantilever response from PTE makes its application to FMM favorable.

PTE FMM experiments were undertaken on a suspended (20 ± 2) μm long, (800 ± 100) nm wide, (200 ± 50) nm thick silicon microbridge[14] with a commercial AFM (Cypher,[20] Asylum Research, Santa Barbara, CA). On the bridge, k varies from $\approx$0.1 N/m to $\approx$1000 N/m. The value of k is independent of f for $f \ll 5$ MHz, the first resonance frequency of the bridge. The measurements were made with gold-coated silicon cantilevers (NCLAu, Nanosensors, Switzerland) with a nominal static bending stiffness $k_L = (40 \pm 10)$ N/m, nominal length $L = (225 \pm 10)$ μm, and a nominal first free flexural resonance frequency of $f_{1,\text{free}} = (150 \pm 20)$ kHz. The actual value of k_L for the specific cantilever used in each experiment was determined with the corrected thermal method.[15] The wavelength of the AFM detection laser was 860 nm, with a spot size of $\approx$30 μm long and $\approx$15 μm wide. The wavelength of the PTE drive laser (blueDrive, Asylum Research, Santa Barbara, CA) was 405 nm with a spot diameter of $\approx$5 μm. The PTE drive laser was supplied with an oscillating power of 9 mW and a constant offset power of 10 mW. The positions of both the detection laser and the drive laser on the cantilever were controlled electronically and monitored optically.

Fig. 2(a) shows an AFM topography image of the silicon microbridge, and Figs. 2(b), 2(c), and 2(d) show PTE FMM maps of A with the drive laser positioned at $x/L \approx 0.5$ and the detection laser positioned at $x/L \approx 0.9$, $x/L \approx 0.2$, and $x/L \approx 0.45$, respectively. The variable x represents position along the length of the cantilever measured from the cantilever base. In Figs. 2(b) and 2(c), A varies monotonically as a function of k. Figs. 2(b) and 2(c) show an inversion of contrast, with A increasing towards the more compliant portion of the bridge in Fig. 2(b) and decreasing in Fig. 2(c). In Fig. 2(d), the relationship between A and k is non-monotonic. For acoustic FMM, A is expected to decrease on more compliant sections of the sample and increase on stiffer sections. For a force applied directly to the cantilever tip, A should increase on compliant sections of the sample and decrease on stiffer sections of the sample. For acoustic and tip-forced FMM, these responses are independent of detector laser position and described by the equations $k/k_L = \frac{1}{A_{\text{stiff}}/A - 1}$ and $k/k_L = A_{\text{free}}/A - 1$, respectively, where A_{stiff} is the cantilever vibration amplitude on an infinitely stiff sample, and A_{free} is the free vibration amplitude of the cantilever.[5,16] The dependence of relative A contrast in PTE FMM on laser positioning indicates that classical FMM analysis fails to describe PTE FMM. We hypothesize that this is because of the location and distribution of force that PTE applies to the cantilever.

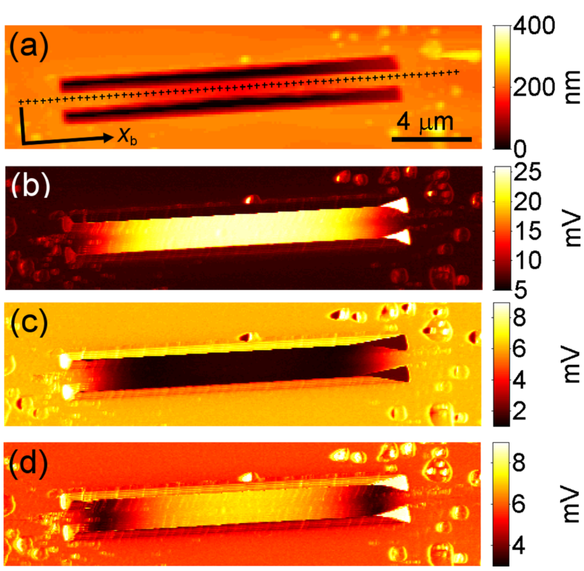

FIG. 2. (a) AFM topography image of microbridge test structure. x_b denotes position along the length of the bridge. (b), (c), and (d) are photothermal force modulation amplitude (photodiode voltage) maps of the microbridge taken at $f/f_{1,\text{free}} = 0.1$ with the drive laser at $x/L \approx 0.5$ and the detection laser at $x/L \approx 0.9$, $x/L \approx 0.2$, and $x/L \approx 0.45$.

Static beam theory predicts that a force applied to the cantilever far below its first resonance will result in a quasi-static vibration shape given by: $EI \frac{\partial^4 w}{\partial x^4} = F(x)$, where E is the Young's modulus of the cantilever, I is the moment of inertia of the cantilever, $w(x)$ is the displacement of the cantilever, and $F(x)$ is the force applied to the cantilever. Solutions of this equation for a concentrated force applied at the tip of the cantilever, a displacement at the base of the sample, or a displacement at the base of the cantilever match exactly the classic FMM configurations described above. For a force distributed along the length of the cantilever or a concentrated moment applied to the cantilever, the cantilever response deviates substantially from the classic FMM solution.

To investigate how forcing affects the quasi-static cantilever response, a recently developed vibrational-shape measurement technique was utilized.[17] By moving the position of the cantilever tip along the microbridge, the evolution of the shape versus k was observed. Vibrational shape measurements were made at 60 positions along the microbridge. While in contact with the sample surface, the deflection feedback loop was turned off and a feedback loop that adjusted the Z-piezo voltage to keep the closed loop Z-sensor at a fixed location was turned on. The Z-sensor setpoint was adjusted during the experiment based on the characteristic drift of the AFM system. In the case of acoustic excitation, the rigid-body-motion of the freely vibrating cantilever detected by the photodiode was subtracted from the measured signal to recover the vibration shape of the cantilever.

Fig. 3 shows quasi-static vibration shapes at $f/f_{1,\text{free}} = 0.1$ for acoustic excitation at the base of the cantilever and for PTE with the drive laser positioned at $x/L \approx 0.1$ and $x/L \approx 0.5$. Each column in each subfigure in Fig. 3 represents a normalized A shape. At each bridge position, the maximum A along the length of the cantilever has been normalized to one. For acoustic excitation shown in Fig. 3(c), the quasi-static cantilever vibration shape is independent of bridge position. For the two PTE cases in Figs. 3(a) and 3(b), the quasi-static cantilever vibration shape depends on bridge position and the location of the drive laser. A consequence of the changing vibrational shape with bridge position, and hence k, is that the optical lever sensitivity and the dynamic stiffness of the cantilever change.

The cantilever vibration shape measurement in Fig. 3(b) allows interpretation of the contrast observed in the PTE FMM A maps in Fig. 2. When the detection laser is at $x/L \approx 0.9$, larger A is observed near the center of the bridge.

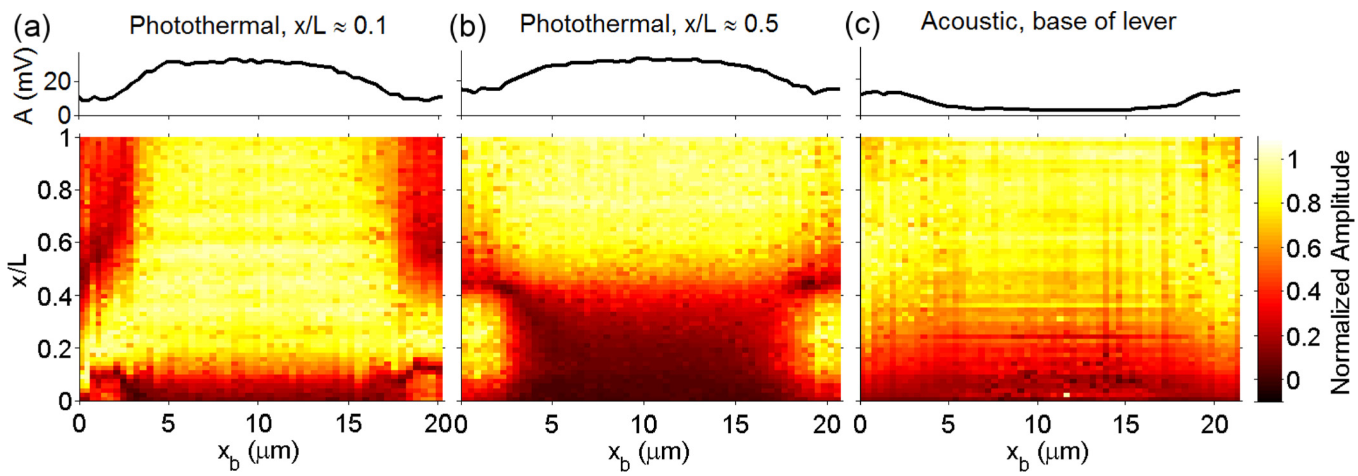

FIG. 3. Quasi-static cantilever amplitude vibration shape at $f/f_{1,\mathrm{free}} = 0.1$ on the suspended bridge structure. (a) and (b) Results for photothermal excitation (PTE) with the drive laser positioned at $x/L \approx 0.1$ and $x/L \approx 0.5$, respectively. (c) Result for acoustic excitation applied at the base of the cantilever. For each x_b, the amplitude is normalized such that the maximum value is one. The line at the top of each subfigure shows this normalization parameter.

When the detection laser is at $x/L \approx 0.2$, larger A is observed near the edge of the bridge. When the detection laser is at $x/L \approx 0.45$, a local minimum in A is crossed at $x_b = 3\,\mu$m and $x_b = 17\,\mu$m. These observations correspond with the contrast observed in Fig. 2(b), demonstrating it is possible to get rank-order k contrast in PTE FMM by careful positioning of the detection and drive lasers to ensure a monotonic A response versus k.

To quantitatively relate A to k, PTE FMM requires reconsideration of the FMM governing equations. Consider a quasi-statically vibrating cantilever with two sets of boundary conditions (BCs). In one case, the cantilever is freely vibrating, and in the other case, the cantilever is in contact with a spring of stiffness k at $x = L$, as shown in Fig. 1(a). If $F(x)$ is the same in both the freely vibrating and contact case, beam theory gives

$$EI\frac{\partial^4 w_c}{\partial x^4} = EI\frac{\partial^4 w_f}{\partial x^4} = F(x), \tag{1}$$

where $w_c(x)$ is the displacement of the cantilever while vibrating in contact with the surface and $w_f(x)$ is the displacement of the cantilever while freely vibrating. The BCs associated with Eq. (1) are: $w_f(0) = 0$, $\frac{\partial w_f}{\partial x}|_{x=0} = 0$, $\frac{\partial^2 w_f}{\partial x^2}|_{x=L} = 0$, $\frac{\partial^3 w_f}{\partial x^3}|_{x=L} = 0$, $w_c(0) = 0$, $\frac{\partial w_c}{\partial x}|_{x=0} = 0$, $\frac{\partial^2 w_c}{\partial x^2}|_{x=L} = 0$, and $EI\frac{\partial^3 w_c}{\partial x^3}|_{x=L} = kw_c(L)$. Replacing EI with $k_L L^3/3$, integrating Eq. (1) four times, and inserting BCs as appropriate results in the expression

$$\frac{k}{k_L} = \frac{\int_0^L \frac{\partial w_f}{\partial x}dx}{\int_0^L \frac{\partial w_c}{\partial x}dx} - 1. \tag{2}$$

Replacing $\frac{\partial w}{\partial x}$ with $A(x)\cos(P(x))$ in Eq. (2), where $P(x)$ is the phase of cantilever oscillation, allows us to convert Fig. 3 into k values.

One additional integration of Eq. (2) leads to a result in terms of displacement that is identical to the classical tip-forced FMM solution. In classic FMM, the displacement can be determined by the standard calibration approach based on the known displacement of the Z-piezo.[1] For PTE-FMM, the cantilever deflection shape during such a calibration is not representative of the cantilever vibrational shape, and thus, the standard calibration is not applicable. Eq. (2) does not require a calibration factor because the optical lever system employed on most AFM systems is a slope sensitive detector, and Eq. (2) is expressed in terms of a ratio of slopes.

Values of k predicted by Eq. (2) are shown in Figs. 4(a) and 4(b) for PTE FMM with the drive laser located at $x/L \approx 0.1$ and $x/L \approx 0.5$. A shape-based FMM analysis has been applied to acoustic excitation in Fig. 4(c). Between $f/f_{1,\mathrm{free}} = 0.02$ and $f/f_{1,\mathrm{free}} = 0.1$ and for $k/k_L < 10$, the average over x_b of k varies by less than 21% with respect to f for base excited PTE, 9% for center excited PTE, and 9% for acoustic excitation. This result illustrates the broadband potential of the PTE FMM technique. Above $f/f_{1,\mathrm{free}} = 0.1$, inertial effects due to resonance become significant, and a quasi-static analysis becomes invalid. Figs. 4(d) and 4(e) show line profiles taken from Figs. 4(a) to 4(c) at $f/f_{1,\mathrm{free}} = 0.1$. The line profiles show good agreement between different excitation types across most of the bridge; however, drift during the experiment makes absolute comparisons at a given bridge location difficult.

To address drift, Fig. 4(f) compares k determined with the shape-based FMM analysis to the stiffness k_{CR} simultaneously determined by contact resonance (CR) force microscopy.[18] Up to $k/k_L = 10$, k and k_{CR} agree to within a factor of 2. Agreement could likely be improved with a more sophisticated beam model; however, the k_{CR} values still serve the purpose of normalizing the FMM data for comparison between excitation methods. A log weighted equivalence analysis (two one-sided t-test) with a significant difference of 20% applied to the ratio of k/k_{CR} shows that the shape-based analysis gives equivalent results ($p = 0.008$) for the different excitation types up to $k/k_L = 10$.

Combining photothermal excitation with force modulation microscopy provides a pathway for broadband nanomechanical property measurements. The technique has been tested in the frequency insensitive bandwidth of a microbridge structure. The developed method can be applied to viscoelastic frequency dependent materials; however, interpretation

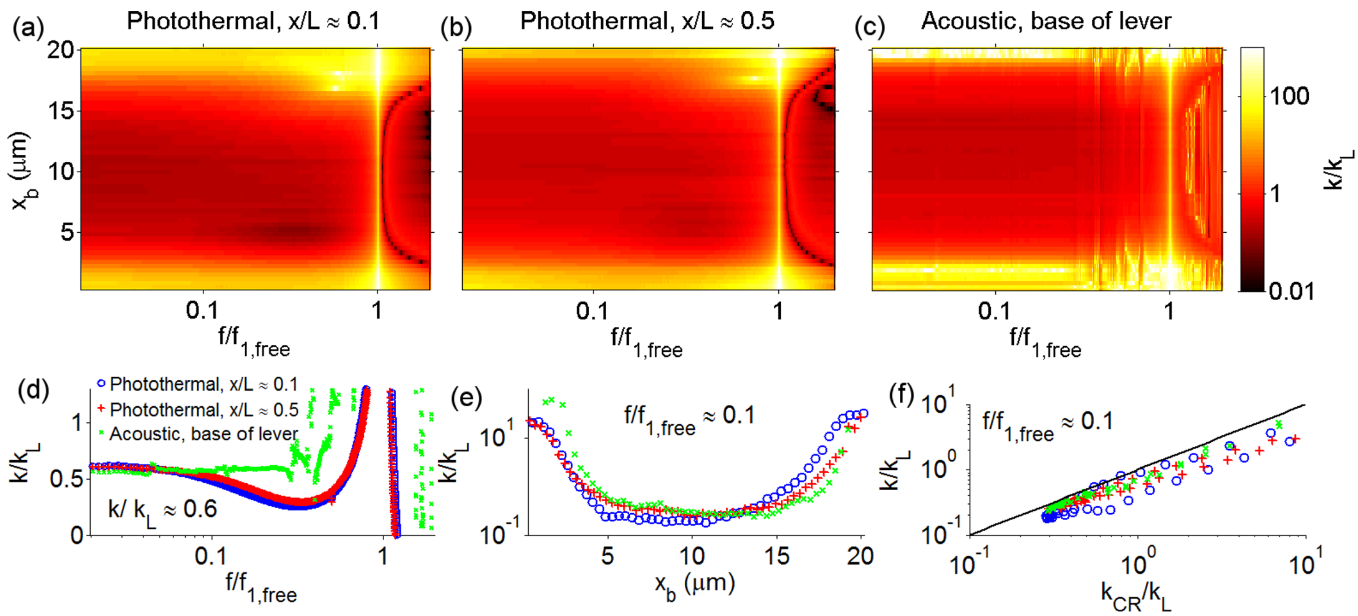

FIG. 4. Shape-based force modulation microscopy results on the microbridge sample. (a) Photothermal excitation (PTE) with the drive laser at $x/L \approx 0.1$. (b) PTE with the drive laser at $x/L \approx 0.5$. (c) Acoustic excitation applied at the base of the cantilever. (d) Selected line profiles versus drive frequency. (e) Selected line profiles along the length of the cantilever. (f) Comparison of contact stiffness determined by FMM to contact stiffness determined by contact resonance force microscopy.

of those results may require consideration of additional effects such as tip-sample creep and differences in environmental damping between free and surface-coupled cantilever configurations. With the smoothly varying transfer function of PTE, the measurement frequency range can be increased by increasing the resonance frequency of the cantilever.[19] This is not an option with acoustic excitation due to spurious vibrations. PTE FMM can produce rank-order amplitude versus stiffness contrast with careful placement of the excitation and detection lasers. Quantitative measurements of stiffness require that the vibrational shape of the photothermally excited cantilever be taken into account. Here, we have demonstrated this shape-based correction on a suspended bridge structure, enabling quantitative PTE FMM.

This work was performed while Ryan Wagner held a National Research Council Associateship Award at NIST.

[1]H.-J. Butt, B. Cappella, and M. Kappl, Surf. Sci. Rep. **59**, 1 (2005).
[2]R. García and R. Pérez, Surf. Sci. Rep. **47**, 197 (2002).
[3]T. Igarashi, S. Fujinami, T. Nishi, N. Asao, and K. Nakajima, Macromolecules **46**, 1916 (2013).
[4]M. Chyasnavichyus, S. L. Young, and V. V. Tsukruk, Langmuir **30**, 10566 (2014).
[5]P. Maivald, H. J. Butt, S. A. C. Gould, C. B. Prater, B. Drake, J. A. Gurley, V. B. Elings, and P. K. Hansma, Nanotechnology **2**, 103 (1991).
[6]G. Meyer and N. M. Amer, Appl. Phys. Lett. **53**, 1045 (1988).
[7]N. Yang, K. K. H. Wong, J. R. de Bruyn, and J. L. Hutter, Meas. Sci. Technol. **20**, 025703 (2009).
[8]Y. Martin and H. K. Wickramasinghe, Appl. Phys. Lett. **50**, 1455 (1987).
[9]T. E. Schäffer, J. P. Cleveland, F. Ohnesorge, D. A. Walters, and P. K. Hansma, J. Appl. Phys. **80**, 3622 (1996).
[10]U. Rabe, S. Hirsekorn, M. Reinstädtler, T. Sulzbach, C. Lehrer, and W. Arnold, Nanotechnology **18**, 044008 (2007).
[11]T. Tsuji, K. Kobari, S. Ide, and K. Yamanaka, Rev. Sci. Instrum. **78**, 103703 (2007).
[12]N. Umeda, S. Ishizaki, and H. Uwai, J. Vac. Sci. Technol. B **9**, 1318 (1991).
[13]D. Kiracofe, K. Kobayashi, A. Labuda, A. Raman, and H. Yamada, Rev. Sci. Instrum. **82**, 013702 (2011).
[14]R. Wagner, J. P. Killgore, R. C. Tung, A. Raman, and D. C. Hurley, Nanotechnology **26**, 045701 (2015).
[15]R. Proksch, T. E. Schäffer, J. P. Cleveland, R. C. Callahan, and M. B. Viani, Nanotechnology **15**, 1344 (2004).
[16]E.-L. Florin, M. Radmacher, B. Fleck, and H. E. Gaub, Rev. Sci. Instrum. **65**, 639 (1994).
[17]R. Wagner, A. Raman, and R. Proksch, Appl. Phys. Lett. **103**, 263102 (2013).
[18]U. Rabe, K. Janser, and W. Arnold, Rev. Sci. Instrum. **67**, 3281 (1996).
[19]D. A. Walters, J. P. Cleveland, N. H. Thomson, P. K. Hansma, M. A. Wendman, G. Gurley, and V. Elings, Rev. Sci. Instrum. **67**, 3583 (1996).
[20]Certain commercial equipment are identified in this paper to foster understanding. Such identification does not imply recommendation or endorsement by NIST, nor does it imply that the equipment identified is necessarily the best available for the purpose.